Acta Biomaterialia xxx (xxxx) xxx



Contents lists available at ScienceDirect

# Acta Biomaterialia

journal homepage: www.elsevier.com/locate/actbio



Full length article

# Revealing chemistry-structure-function relationships in shark vertebrae across length scales

Dawn Raja Somu<sup>a</sup>, Malena Fuentes<sup>a</sup>, Lihua Lou<sup>b</sup>, Arvind Agarwal<sup>b</sup>, Marianne Porter<sup>c</sup>, Vivian Merk<sup>a,\*</sup>

- <sup>a</sup> Department of Chemistry and Biochemistry, Department of Ocean and Mechanical Engineering, Florida Atlantic University, Boca Raton, FL 33431, USA
- <sup>b</sup> Department of Mechanical and Materials Engineering, Florida International University, Miami, FL 33174, USA
- <sup>c</sup> Department of Biological Sciences, Florida Atlantic University, Boca Raton, FL 33431, USA

#### ARTICLE INFO

#### Article history: Received 29 April 2024 Revised 22 September 2024 Accepted 24 September 2024 Available online xxx

Keywords:
Biomineralization
Cartilage
Bioapatite
Atomic force microscopy
Raman microscopy
Nanoindentation
Polarized light microscopy

#### ABSTRACT

Shark cartilage presents a complex material composed of collagen, proteoglycans, and bioapatite. In the present study, we explored the link between microstructure, chemical composition, and biomechanical function of shark vertebral cartilage using Polarized Light Microscopy (PLM), Atomic Force Microscopy (AFM), Confocal Raman Microspectroscopy, and Nanoindentation. Our investigation focused on vertebrae from Blacktip and Shortfin Mako sharks. As typical representatives of the orders Carcharhiniformes and Lamniformes, these species differ in preferred habitat, ecological role, and swimming style. We observed structural variations in mineral organization and collagen fiber arrangement using PLM and AFM. In both sharks, the highly calcified corpus calcarea shows a ridged morphology, while a chain-like network is present in the less mineralized intermedialia. Raman spectromicroscopy demonstrates a relative increase of glucosaminocycans (GAGs) with respect to collagen and a decrease in mineral-rich zones, underlining the role of GAGs in modulating bioapatite mineralization. Region-specific testing confirmed that intravertebral variations in mineral content and arrangement result in distinct nanomechanical properties. Local Young's moduli from mineralized regions exceeded bulk values by a factor of 10. Overall, this work provides profound insights into a flexible yet strong biocomposite, which is crucial for the extraordinary speed of cartilaginous fish in the worlds' oceans.

## Statement of significance

Shark cartilage is a morphologically complex material composed of collagen, sulfated proteoglycans, and calcium phosphate minerals. This study explores the link between microstructure, chemical composition, and biological mechanical function of shark vertebral cartilage at the micro- and nanometer scale in typical Carcharhiniform and Lamniform shark species, which represent different vertebral mineralization morphologies, swimming styles and speeds. By studying the intricacies of shark vertebrae, we hope to lay the foundation for biomimetic composite materials that harness lamellar reinforcement and tailored stiffness gradients, capable of dynamic and localized adjustments during movement.

© 2024 Acta Materialia Inc. Published by Elsevier Ltd. All rights are reserved, including those for text and data mining, AI training, and similar technologies.

#### 1. Introduction

Nature serves as an inspirational framework for the design and development of composite materials, and the applications for such bioinspired materials are far-ranging in the fields of tissue engineering, general biomedicine, marine robotics, and more [1–8]. One example of a robust and flexible biomaterial is the verte-

\* Corresponding author. E-mail address: vmerk@fau.edu (V. Merk). bral cartilage of sharks. Sharks evolved over 450 million years ago, and their cartilaginous endoskeletons are fine-tuned and optimized for aquatic locomotion [9,10]. Sharks entirely lack bone and instead build skeletons from mineralized cartilage. Their cartilaginous endoskeleton is a biological composite material comprised of a matrix of collagen fibers (mainly type II), proteoglycans, and, in calcified cartilage, hydroxyapatite mineral [11–13]. The vertebral column of sharks works as a central spring that absorbs and releases energy as they swim [12,14,15]. Functional structure and macroscale mechanical properties of shark vertebral

https://doi.org/10.1016/j.actbio.2024.09.041

1742-7061/© 2024 Acta Materialia Inc. Published by Elsevier Ltd. All rights are reserved, including those for text and data mining, Al training, and similar technologies.

D. Raja Somu, M. Fuentes, L. Lou et al.

Acta Biomaterialia xxx (xxxx) xxx

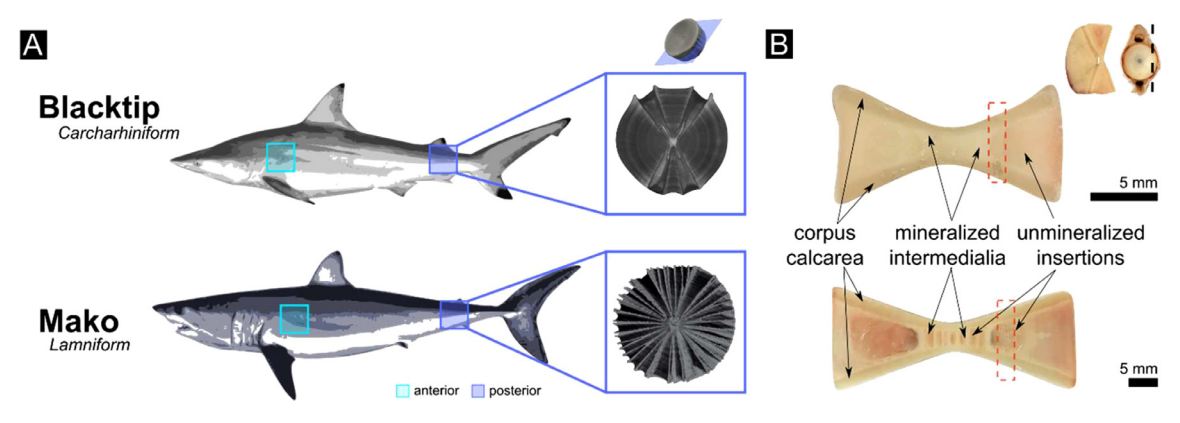


Fig. 1. A) Blacktip shark (Carcharhiniform) and Shortfin Mako shark (Lamniform). The approximate regions from which vertebrae were obtained are highlighted. Insets: Labsource microCT scans illustrate differences in vertebral mineralization patterns. The centra are composed of double-cone shaped corpus calcarea, which cover unmineralized arches and intermedialia on side of the cranio-caudally oriented centra. The notochord remnant can be seen in the center of each centrum, as shown in the transverse cross-sections. (B) Typical sections from sagittal cut (inset) on whole vertebral centra from Blacktip and Shortfin Mako sharks showing interspecific differences in vertebral cartilage structure. Red dotted lines show typical cuts made for further sample preparation. Images of sharks in (A) adapted from [26].

cartilage can show great variety among species, along the length of an individual's vertebral column, and within individual vertebrae [12,14,16,17].

Previous studies reported on the extensive morphological variation in vertebral mineralization patterns between shark species [12,14,16,17]. In this work, we compare selected species from two orders of sharks: Blacktip shark (Carcharhinus limbatus) from the order Carcharhiniformes (ground sharks) and Shortfin Mako shark (Isurus oxyrhincus) from the order Lamniformes (mackerel sharks) (Fig. 1). Sharks from these two orders differ in terms of preferred habitat, ecological role, and swimming style. Requiem sharks, of the Carcharhinidae family under the Carcharhiniform order, are generally found in epibenthic warm waters along coastal regions [18-20]. These sharks adopt a carangiform mode of swimming, in which the wave-like movement that propels the shark forward is concentrated towards the posterior region of its body. Blacktip sharks, in their natural swimming habitat, employ a doubleoscillatory movement, such that the anterior and posterior regions of the vertebral column can move independently about the central body axis [21]. Lamnid sharks, on the other hand, employ the thunniform swimming mode, in which the body wavelengths necessary for forward propulsion are produced near the caudal peduncle [22]. This powerful mode of swimming is fueled in part by regional endothermy, in which lamnids are capable of localized thermoregulation, maintaining higher core temperatures compared to other types of sharks [23,24]. Hydrodynamic analyses of thunniform swimming models show that fish of this type can reach high speeds of steady-rate swimming whilst maintaining excellent swimming efficiency [25]. The extent to which the posterior region of the body is used, and the method in which it bends, varies across shark species [24].

Shark vertebral centra can be classified into three major regions, as shown in Fig. 1B and Fig. S1. The highly calcified corpus calcarea, comprising of the double-cone structure surrounding the top and bottom of the centra, covers the mineralized intermedialia and unmineralized gaps. The vertebrae of Carcharhiniformes showcase block-like mineralization patterns, with the neural and hemal arches inserted and extended into the center as unmineralized spaces. Lamniformes have morphologically complex vertebrae, which feature radiating lamellae with alternating mineralized and unmineralized regions [11–13]. Previous studies have explored the structure, composition, and hierarchical organization of tessellated cartilage in elasmobranchs in-depth, and a few recent studies have characterized certain aspects of shark vertebral cartilage [27–

33]. However, there is still much that is unknown about vertebral cartilage. Macroscale material properties of bulk vertebral cartilage have been studied in-depth in various shark species and show that the vertebrae centra containing a higher degree of mineralization exhibit a high elastic modulus in bulk mechanical testing [14]. However, a deeper examination of the material that composes shark vertebral cartilage is necessary to probe into the reason behind its enhanced mechanical properties. For instance, the spatial distribution of minerals within different regions of the shark vertebrae and their corresponding nanomechanical properties are yet to be explored.

In this paper, we investigate the hierarchical organization, chemical composition and region-specific mechanical behavior of shark cartilage and compare results from Blacktip and Shortfin Mako shark. The compositional and ultrastructural foundations of shark cartilage are explored through Polarized Light Microscopy (PLM), Atomic Force Microscopy (AFM), confocal Raman microscopy, and Nanoindentation. We hypothesize that the orientation of the collagen fibers, the micro- and nanoscale mineralization patterns, as well as the density of chondrocytes and lacunar spaces affect local mechanical properties. A comprehensive study of the chemical and nanomechanical properties will help us understand the range of function of the vertebral column, which results in varied swimming styles and speeds in sharks.

# 2. Materials and methods

# 2.1. Sample preparation

Frozen shark vertebrae were obtained for the experiment from collaborators as segments of continuous vertebrae and stored in  $-20^{\circ}\text{C}$  until use. Vertebrae were obtained from four blacktip sharks (*Carcharhinus limbatus*) and three mako sharks (*Isurus oxyrinchus*). , as per availability. Information on samples used for each technique is presented in Table S1 and information about individual sharks in Table S2. Individual vertebral centra were left intact as long as possible until sample preparation. Neural and hemal arches were excised from the vertebral centra. Vertebrae were cut to smaller pieces either by hand with a single-edged razor blade or using a Buehler IsoMet1000 Precision Saw with a 7-inch 15HC IsoMet Diamond Blade at a speed of 100 rpm, depending on the size of the centrum. Samples that were cut, if not used immediately, were stored in elasmobranch Ringer's solution in the freezer until further use.

D. Raja Somu, M. Fuentes, L. Lou et al. Acta Biomaterialia xxx (xxxx) xxx

#### 2.2. Embedding process

Samples were fixed in 2.5 % glutaraldehyde in  $H_2O$  overnight and then dehydrated in a series of ethanol solutions (50 %, 70 %, 90 %, 100 %,  $2\times$  and 10 min each). Samples were then transferred to propylene oxide ( $2\times$ , 15 min each), then to a 1:1 propylene oxide:EMbed812 resin mixture (without hardener) for an hour, and a 1:2 propylene oxide:EMbed812 resin mixture (without hardener) after that and left overnight. The EMbed 812 kit for electron microscopy embedding (Electron Microscopy Sciences, Hatfield, PA, USA) was used, following the "medium" hardness formulation. Samples were then transferred to a 100 % resin mixture (without hardener) and underwent five 15-min vacuum/release cycles, after which the samples remained under vacuum overnight. Samples were cut to the required size, and then transferred to molds with a fresh batch of resin and DMP-30 hardener and cured in the oven at  $60^{\circ}$ C (1-2 days).

#### 2.3. Polarized light microscopy

Freshly thawed samples of shark vertebrae were cut into 20–40 µm slices using a Leica RM2125RTS rotary microtome. Slices were placed under a coverslip and viewed using a Leica M125 C stereoscope with a polarizing plate and analyzer attachment. Bright field and dark field images were collected using a Leica DMC6200 digital microscope camera. Further fiber directionality analysis of selected images was carried out using ImageJ's Directionality plugin.

#### 2.4. Atomic force microscopy

750 nm thick slices were collected from resin-embedded samples using a Leica Ultracut EM UC7RT ultramicrotome and glass knives made using the Leica EM KMR3 glass knifemaker. Slices were placed on a glass substrate for imaging. Samples were characterized using an AFM Workshop TT-2 atomic force microscope, with 50 µm and 15 µm scanners. Samples were scanned in tapping mode using AFM Workshop ACLA-10-W probes with a rectangular Sb-doped Si cantilever with reflective Al coating. Drive and phase images were collected for each sample. Embedded samples were used here to obtain very flat regions suitable for microscale examination of shark vertebral cartilage structure using AFM. Images obtained were post-processed using Gwyddion (v. 2.59) software. Standard procedure included mean plane subtraction to level data and removal of polynomial background. The align rows module was further used as necessary.

#### 2.5. Confocal Raman microscopy

20–40 μm thick slices were collected from frozen, unembedded shark vertebrae samples using the rotary microtome and placed under a coverslip with water and sealed to create a make-shift fluid cell. Spectra were collected with a Horiba Xplora Raman microscope, using a 532 nm green laser and a 100× oil objective with a numerical aperture of 1.25. A 600 gr/mm grating and a CCD detector were also used. Obtained mapping data were then background-corrected using the adaptive background correction module in Spectragryph (v1.2.15), and then analyzed using Cytospec (v.2.00.06) software. Background-corrected spectra were vector normalized prior to carrying out cluster analysis. Vertex Components Analysis (VCA) was performed to unmix hyperspectral data and determine three endmember spectra. FWHM maps for the  $\nu_1$  (phosphate) peak at 907–992 cm<sup>-1</sup> were obtained using an interpolation factor of 16.

#### 2.6. Nanoindentation

Unembedded shark vertebral samples were cut and planed using a rotary microtome whilst maintaining either cone-to-cone (parallel to direction of biological strain) or arch-to-arch (perpendicular to direction of biological strain) orientation. Individual pieces were glued to a flat petri dish and immersed with Elasmobranch Ringer's solution prior to data collection. Sample thickness ranged from 0.3 to 2.5 cm, much thicker than the expected indentation depth. Nanoindentation measurements were obtained using a Hysitron BioSoft nanoindenter with a 0.1 µm radius Berkovich tip. Nanoindentation data was collected in load-control mode. Indentation protocol consisted of a loading segment with a loading rate of 50  $\mu N/s$  and maximum load of 1000  $\mu N$ , an unloading segment at - 50  $\mu N/s$  up to -1000  $\mu N$ , and a retraction step at  $-2 \mu m/s$  for 10 s. Samples were assumed to have a Poisson's ratio of 0.3 for further analysis. A Hertzian model was applied, and the elastic modulus was determined for each measured curve. Statistical analyses were carried out using OriginPro software (v. 2022). Around 10-20 measurements were obtained for each dataset; details are presented in Table S4 and S5. Outlier data were identified and removed using the interquartile range (IQR) method, where IQR is defined as the range between the first quartile (Q1) and the third quartile (Q3). Data points falling fall below Q1 -  $1.5 \times IQR$ or above Q3 + 1.5  $\times$  IQR were considered outliers and excluded to ensure data consistency.

#### 2.7. Statistical analysis

Statistical analyses were carried out using OriginPro software (v. 2022). We used nonparametric statistics as only 10 out of 24 datasets failed to reject normality as determined using Shapiro-Wilk tests. Nonparametric Kruskal-Wallis ANOVA followed by post-hoc Dunn tests were carried out at a 0.05 significance level to determine whether means in each group (data from anterior and posterior vertebrae of both sharks for each combination of region (corpus calcarea/mineralized intermedialia/unmineralized insertions) and direction (parallel/perpendicular)) were significantly different.

### 3. Results and discussion

# 3.1. Polarized light microscopy

The intrinsic birefringent properties of ordered collagen allow for the examination of collagen-rich shark vertebral cartilage using polarized light microscopy. Fig. 2 shows polarized light micrographs taken of posterior vertebral cartilage from Blacktip and Shortfin Mako sharks. We found stark differences in the organization of collagen in the unmineralized gaps between the two sharks. Across the intermedialia and the unmineralized insertions, there was a uniform distribution of fibrillar collagen bundles in Mako vertebrae that was absent in that of the Blacktip shark. At the mineralized-unmineralized interface of Blacktip shark cartilage we see more obviously the presence of the chondrocyte cells and layers of collagen under polarized light. However, in thinner slices of around 3 µm, there is no apparent long-range arrangement of the collagen fibers in the Blacktip shark and the clear fibrillar arrangement prevalent in Mako sharks is absent (Fig. S2). Recently, Stock et al. observed a preferred collagen fiber orientation in unstained Blue and Mako shark cartilage under polarized light [34]. These structural differences within different regions of the vertebra were explored further using atomic force microscopy. Similar features were observed in sections obtained in directions perpendicular to those in Fig. 1 (Fig. S3).

D. Raja Somu, M. Fuentes, L. Lou et al.

Acta Biomaterialia xxx (xxxx) xxx

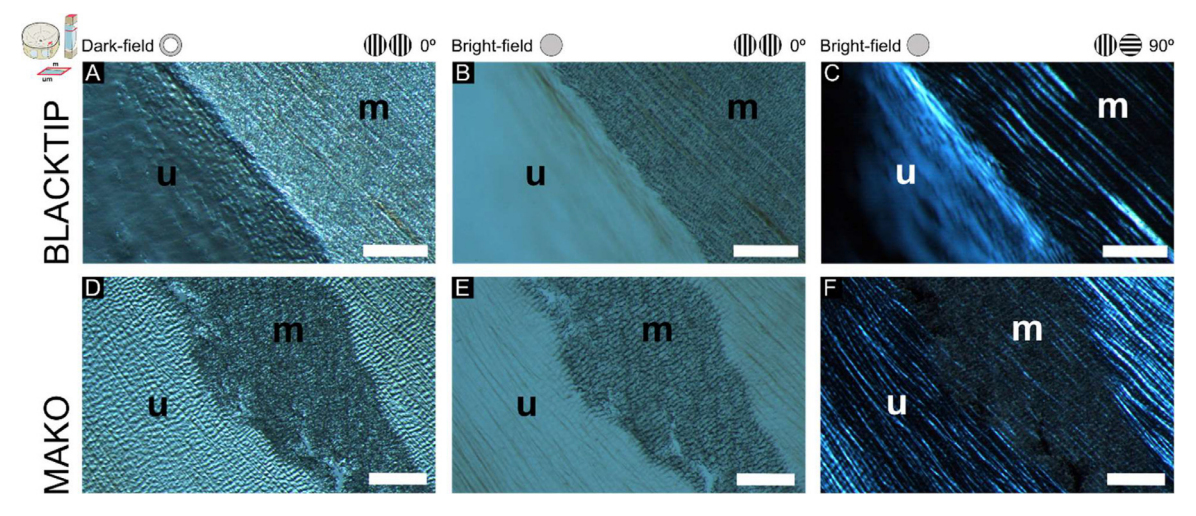


Fig. 2. Low-angle dark-field (A,D) and bright-field (B and C, E and F) polarized light micrographs of the interface between mineralized intermedialia, m, and unmineralized insertions, u, in Blacktip (A–C) and Mako (D–F) sharks. Angle between polarizing plate and analyzer indicated for each column. Inset: Illustration shows how slices were obtained. Scalebars equal 200 μm.

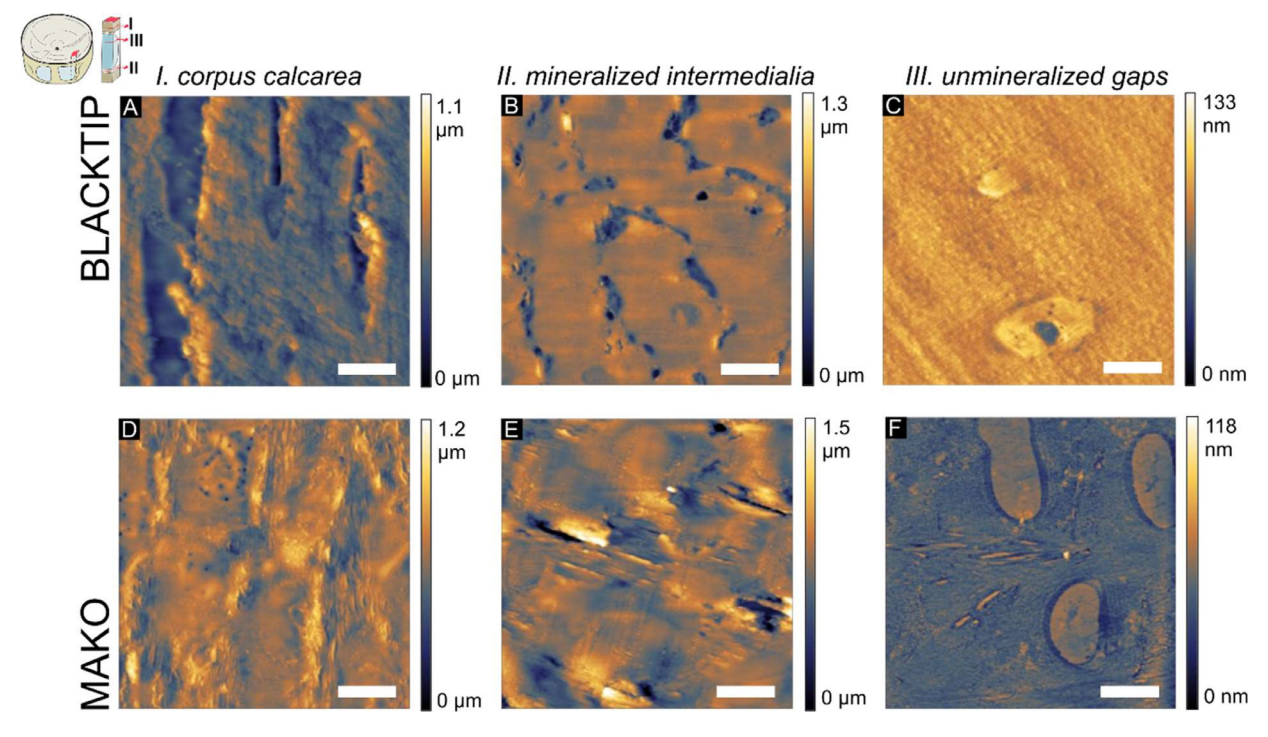


Fig. 3. Different regions of vertebral cartilage from Blacktip and Mako sharks examined using Atomic Force Microscopy. Illustration shows how slices were obtained. Scalebars equal 10 μm.

#### 3.2. Atomic force microscopy

The structural differences between the corpus calcarea, mineralized, and unmineralized regions of posterior vertebrae of Blacktip shark and Mako shark, as examined using AFM, are presented in Fig. 3. In both sharks, the corpus calcareum shows a ridged morphology and an overall thicker mineralized network compared to the intermedialie. Especially, the denser oriented network in the Blacktip vertebrae corroborates with previous microCT studies, where the corpus calcarea appeared brighter due to its greater linear attenuation coefficient compared to the intermedialia [33,35]. The intermedialia of both samples appear to have a chain-like woven network of mineralized fibers, which could be beneficial for dissipating stress away from points of compression, minimizing point fractures. Network structures, such as open-cell foams or

honeycomb structures, are known to be advantageous for energy dissipation [36,3]. The unmineralized regions of the two sharks, however, are strikingly different, especially evidenced by the presence of needle-like fiber bundles throughout this regime in Short-fin Mako (Figs. 3F, 4 and S7), which is consistent with the uniformly distributed fibrillar collagen bundles visible in polarized light microscopy (Fig. 2). The unmineralized region of the Blacktip shark vertebrae lacks this microstructural feature.

The circular spaces in the unmineralized region of the Mako shark appear to be empty lacunae. The paired space in Fig. 3F especially lends credence to this claim, as it is similar in shape to lacunae in which isogenous chondrocytes are found. The sizes of these lacunae are similar to that of other elasmobranchs [37]. While it is possible that the lacunae in this region are simply empty, contributing to potential poro-viscoelastic behavior of the

D. Raja Somu, M. Fuentes, L. Lou et al.

Acta Biomaterialia xxx (xxxx) xxx

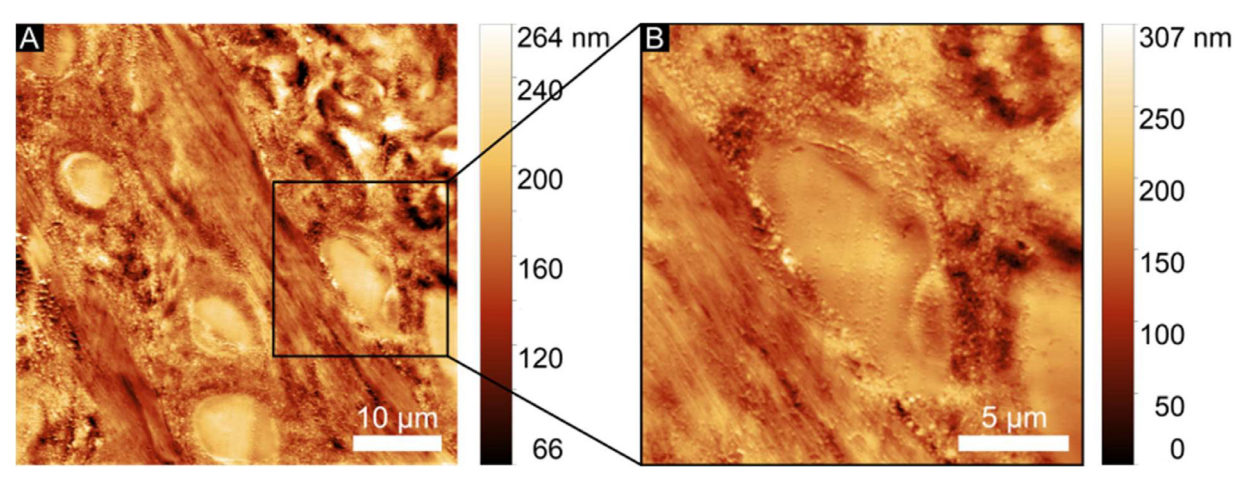


Fig. 4. AFM image of mineralized intermedialia in Mako shark vertebrae showing fibrillar structure of collagen bundles.

Table 1
Major peak assignments in mineralized vertebral cartilage of Blacktip and Mako sharks.

Peak	Assignment	References
430 cm <sup>-1</sup>	$\nu_2(\text{PO}_4)^{3-}$ of apatite	[38]
587 cm <sup>-1</sup>	$v_4(PO_4)^{3-}$ of apatite	[38]
	skeletal C-O-C from sulfated GAGs	[39]
859 cm <sup>-1</sup>	$\nu$ (C–C) proline ring (collagen)	[40,41]
943 cm <sup>-1</sup>	$\nu$ (C-C) hydroxyproline (collagen)	[40]
	C-O-C link skeletal modes GAG	[39]
962 cm <sup>-1</sup>	$v_1(PO_4)^{3-}$ of apatite	[38]
1004–1007 cm <sup>-1</sup>	$\nu_{\rm s}({\rm C-C})$ of phenylalanine collagen	[40]
	$\nu_1({\rm HPO_4})^{2-}$ in apatite	[38]
1073 cm <sup>-1</sup>	$v_s$ (S=0) of GAG (1065 cm <sup>-1</sup> )	[39]
	$\nu_3(PO_4)^{3-}$ of apatite $\sim 1070~cm^{-1}$ if B-type subst. in apatite	[38]
1105 cm <sup>-1</sup>	$\nu_1(\text{CO}_3)^{2-}$ for A-type subst. in apatite	[38]
1250 cm <sup>-1</sup> , 1270 cm <sup>-1</sup>	Amide III $\nu(C-N)$ and $\delta(N-H)$ of collagen	[39,42-44]
1390 cm <sup>-1</sup>	$\delta(CH_2)$ in collagen	[45]
1429 cm <sup>-1</sup>	CH <sub>3</sub> deformation	[44]
1459 cm <sup>-1</sup>	$\nu_{\rm as}$ COO <sup>-</sup> Lys, $\delta({\rm CH_2})$ in collagen	[43]
1671 cm <sup>-1</sup>	Amide I $\nu$ (C=0) of collagen	[40,43-45]

material under stress, it is also possible that they did not hold on to cellular material due to poor fixation prior to embedding or due to cryogenic artefacts.

# 3.3. Confocal Raman microscopy

Raman spectroscopic data of shark vertebrae samples detail compositional variations at the microscopic level. Here, hyperspectral mappings generated by confocal Raman microscopy were obtained from the mineralized intermedialia of a posterior vertebra both from Blacktip (Fig. 5A–C) and Shortfin Mako shark (Fig. 5D–F). Both mappings highlight the overall chain-like fibrous network formed by the mineralized collagen fibers in this region of shark vertebral cartilage. Through vertex component analysis performed on each map, regions of local variation in chemical composition were distinguished. Distribution of the different endmember components and comparison of spectra between the two sharks are also presented in Figs. S5 and S6. Major bands and their associated source within the examined cartilage are presented in Table 1.

The main peaks associated with the presence of apatite at 430 cm<sup>-1</sup>, 587 cm<sup>-1</sup>, 962 cm<sup>-1</sup>, and 1073 cm<sup>-1</sup> assigned to  $\nu_2(PO_4)^{3-}$ ,  $\nu_4(PO_4)^{3-}$ ,  $\nu_1(PO_4)^{3-}$ , and  $\nu_3(PO_4)^{3-}$ , respectively, were present in the mineral network of the intermedialia in both sharks. Bioapatite is made of carbonate-substituted hydroxyapatite, as seen in other naturally found bioapatite sources. Here, the presence of the shoulder at around 1105–1107 cm<sup>-1</sup> could originate from the  $\nu_1(CO_3)^{2-}$ 

band from an A-type carbonate substitution. Previous macroscale mechanical studies of shark vertebrae have shown that the degree of mineralization influences material properties of shark vertebrae, such as stiffness and toughness [12,14]. Major peaks attributed to collagen, such as the 859 cm $^{-1}$ , 1250 cm $^{-1}$  and the 1671 cm $^{-1}$  assigned respectively to the  $\nu(\text{C-C})$  band of the proline ring, the Amide III band ( $\nu(\text{C-N})$  and  $\delta(\text{N-H})$ ), and the Amide I band ( $\nu(\text{C=O})$ ), were present throughout the mineralized networks of both shark species.

Across the cartilage tissue of the vertebral centra, however, there are variations in the amount of mineral and organic material. This is especially evident in the 990–1150 cm<sup>-1</sup> region, where the unmineralized inclusions have a peak at around 1065 cm<sup>-1</sup>, whereas the more mineralized regions in the map have a prominent peak at 1075 cm<sup>-1</sup> (Fig. S5). The 1065 cm<sup>-1</sup> peak is assigned to the O-S-O symmetric stretch from sulfated glucosaminoglycans (GAGs), specifically chondroitin-6-sulfate, present in shark cartilage. While not directly influencing stiffness at the macroscale [12], it is hypothesized that GAGs inhibit cartilage calcification [13,46] in vitro [47] through interaction with sulfate moieties, as well as in biological tissues, such as shark jaw [42] and vertebrae [12]. In the current investigation, Raman spectromicroscopic data is consistent with a relative increase of GAGs with respect to collagen and a decreased abundance of GAGs in mineralrich zones. Apart from modulating mineralization though interfacial adsorption, proteoglycans in human cartilage occasionally intersect with collagen fibrils and act as an interlock across long

Acta Biomaterialia xxx (xxxx) xxx

JID: ACTBIO [m5G;October 14, 2024;16:53]

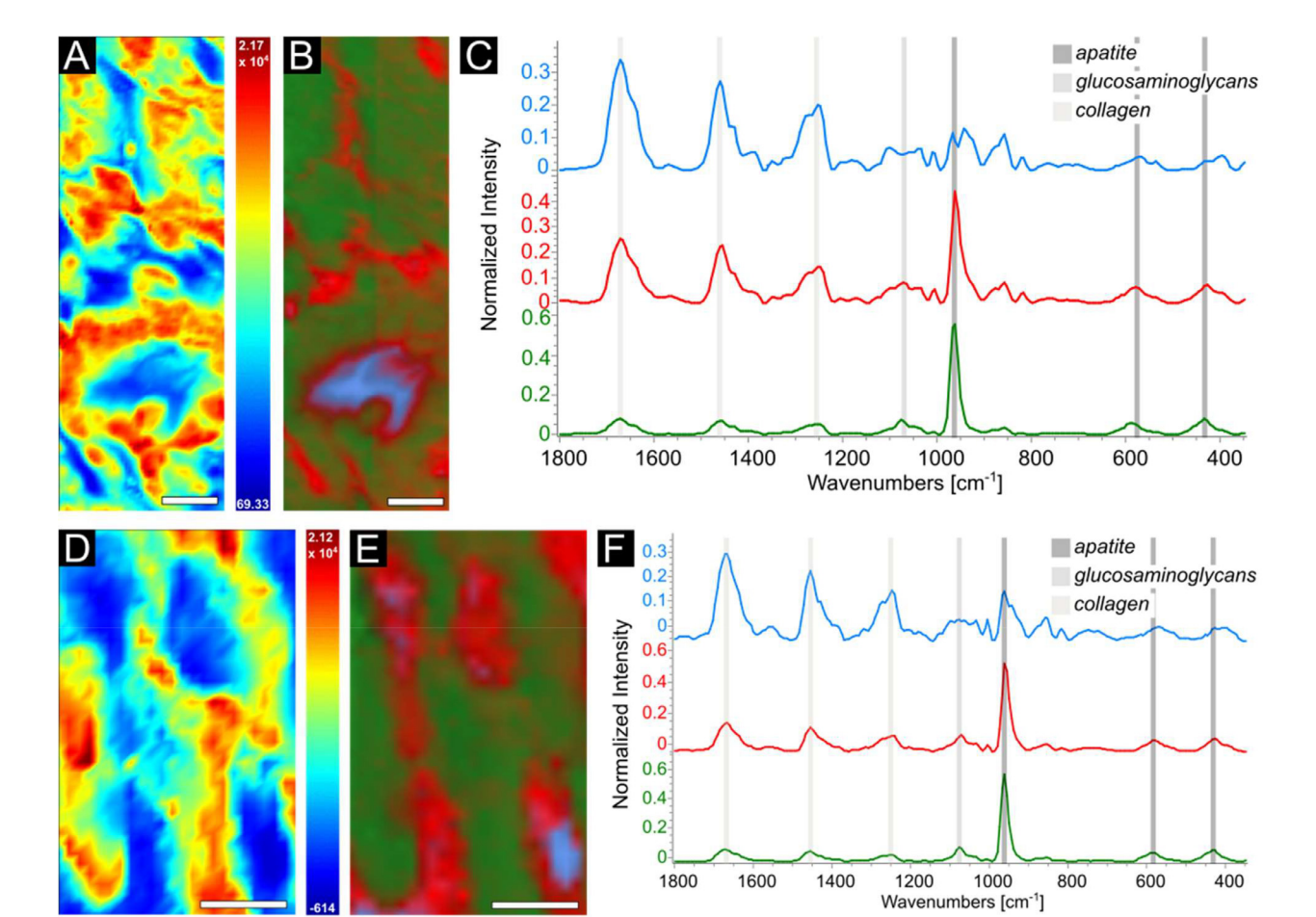


**Fig. 5.** Raman spectroscopy mapping of mineralized cartilage from posterior vertebrae of Blacktip (A-C) and Shortfin Mako (D-F) sharks (A,D). Chemical map of region obtained by integrating peak at 960 cm<sup>-1</sup>, assigned to  $\nu_1(PO_4)^{3-}$  of bioapatite. (B,E) Composite image generated by vertex component analysis of Raman mapping after post-processing spectra, showing relative spatial distribution of three endmembers. (C,F): Endmember spectra from mappings B and E, respectively, highlighting major bands attributed to apatite, glucosaminoglycans, and collagen. Displayed spectra normalized for peak maxima. Scalebars correspond to 10 μm.

distances [48], enabling the tissue to return to its original shape after expansion and boosting energy absorption. Similarly, cross-linking GAGs in shark vertebral cartilage may improve toughness, resulting in a composite material with tunable mechanics.

D. Raja Somu, M. Fuentes, L. Lou et al.

Hoenig and Walsh described the presence of lacunar cartilage canals in several species of sharksding Mako sharks and a few species of Carcharhiniforms [49]. The presence of these canals was further examined by Morse et al., who found the channels to be flanked by microrods on either side [50]. In the present study, we found unmineralized pockets on the order of 20-30 µm, suggesting that either the canals can be much smaller than previously described or that there are other regions of non-mineral material scattered throughout the intermedialia. Such insertions were absent in our examinations of the corpus calcarea regions. It has been hypothesized that the presence of cartilage canals in the intermedialia could serve biological purposes, such as providing nutrition to the inner-cartilage region. The placement and prevalence of the inclusions observed here render it possible that these smaller regions of low mineral content fulfill a mechanical function in addition to serving as local reservoirs of nutrition. Previous research has found that cartilage canals are especially prevalent near the intermedialus-calcareum interface [49], which could be a region that undergoes more stress compared to the deeper regions of the intermedialia during the complex bending motion that sharks undertake during locomotion.

We examined the degree of crystallinity of the mineralized cartilage from the posterior region of both the Mako and Blacktip sharks through mapping the change in the full width at half maximum (FWHM) of the  $\nu_1$  peak of the apatite mineral at  $960~\rm cm^{-1}$ , as seen in Fig. 6. We find that the sparsely mineralized regions as well as the curved areas in the microstructure, towards the edges of mineral-rich regions of cartilage, are less crystalline, as indicated by a greater FWHM. This makes sense, as in the regions where the mineralized network needs to curve, there could be greater stress demand. In-vitro studies show that hydroxyapatite formation is inhibited in the presence of proteoglycans extracted from elasmobranchs [13]. The less-crystalline curved areas in the map have a higher GAG: Apatite ratio (Table S3), supporting the claim GAGs are involved in actively guiding and modulating mineralization of shark vertebral cartilage.

# 3.4. Nanoindentation

We found differences in the local micromechanical properties of the vertebral cartilage of Blacktip and Mako sharks. Here, we examined localized mechanical properties, e.g., elastic modulus, between the two sharks in anterior and posterior vertebrae, measured parallel and perpendicular to the primary direction of biological strain. During swimming, sharks perform complex movements that will expose their vertebrae to multidirectional strain, e.g., bending, torsion, shear, etc. Fig. 7 shows the overall summary of the obtained data. Representative load–displacement curves were used to determine elastic moduli are shown in Supplemental Figs. S8 and S9.

D. Raja Somu, M. Fuentes, L. Lou et al.

Acta Biomaterialia xxx (xxxx) xxx

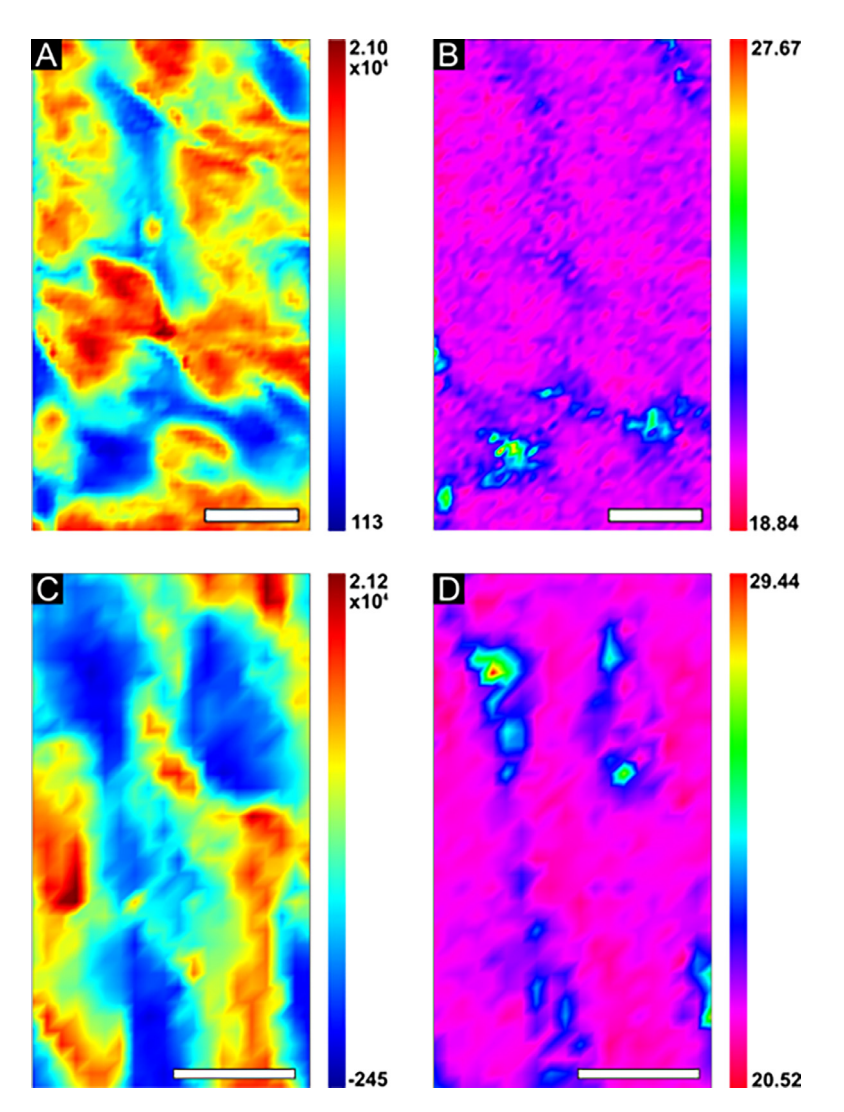


**Fig. 6.** Selected regions from Raman mappings of Blacktip (A and B) and Mako (C and D) were used to examine changes in crystallinity within the mineralized matrix. (A,C) show the chemical map of region obtained by integrating to  $\nu_1(PO_4)^{3-}$  peak from apatite at 960 cm<sup>-1</sup>. (B,D) are maps of the full-width at half maximum (FWHM) for the 960 cm<sup>-1</sup> apatite peak. Scalebars correspond to 10 μm.

We found the unmineralized insertions in the centra to be significantly less stiff, with elastic moduli of at least an order of magnitude lower than the intermedialia and the corpus calcarea, as expected from the absence of hard mineral inclusions. This result applied to both shark species in the anterior and posterior position of the vertebral column, as well as parallel and perpendicular to biological strain. It is noteworthy that the unmineralized regions of Blacktip shark are significantly stiffer than Shortfin Mako when tested parallel to the main direction of biological strain. We conclude that the primary factor resulting in an increase of cartilage stiffness appears to be the presence of apatite mineral in the matrix.

Our nanomechanical data suggest that the corpus calcarea is stiffer in the anterior region of the vertebral column compared to the posterior in Mako shark vertebrae. In anterior vertebrae, it appears that the stiffness of the Mako and Blacktip sharks are not significantly different. However, the cones of the posterior vertebrae of the Mako shark are less stiff than that of the Blacktip shark. Overall, among the three intra-vertebral regions examined here, the corpus calcarea produced the most uniform values for elastic modulus, which could be related to its high degree of calcification. X-radiograph and microCT studies showed a greater linear attenuation coefficient in the cones for Blacktip, indicating a higher

degree of mineralization of the corpus calcarea [33,35]. Since the mineral in this region is more densely arranged compared to the intermedialia, it is possible that the thicker mineral framework is more easily accessible to the indenter tip in both perpendicular and parallel orientations. The stiffness of the mineralized intermedialia in both anterior and posterior regions of both sharks are comparable between the two shark species when measured in the direction parallel to biological strain. In the perpendicular direction, however, vertebral intermedialia in the anterior region of the Mako shark has an elastic modulus of around 2 GPa, which is much stiffer than the posterior region of the Mako shark and the Blacktip shark in both anterior and posterior regions. Previous studies have found that orientation of c-axis in apatite crystals in shark vertebral cartilage in the corpus calcarean and intermedialia are radial and longitudinal, respectively [51]. The previously reported c-axis alignment in apatite is known to play a crucial role in the overall mechanical properties of biological and synthetic composites containing apatite mineral, as composites tend to be stiffer along the direction of alignment [52–55]. We observed a larger variation in elastic moduli when measured in the parallel direction compared to the perpendicular direction. The elastic stiffness of fiber reinforced composites, such as shark vertebral cartilage, also depends on the fiber orientation angle, with the highest elastic modulus

Acta Biomaterialia xxx (xxxx) xxx

JID: ACTBIO [m5G;October 14, 2024;16:53]

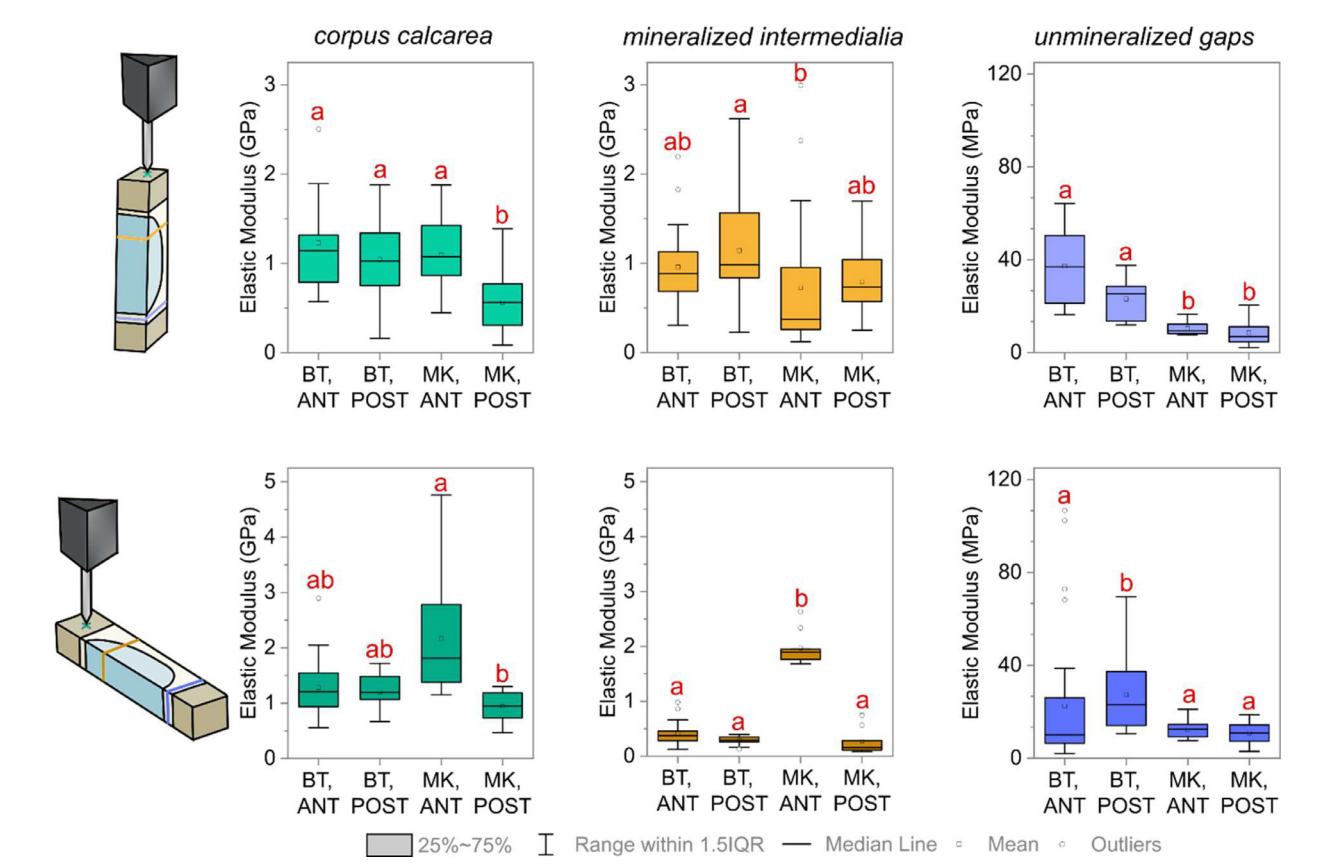


Fig. 7. Box plots showing elastic moduli of different regions of Blacktip (BT) and Shortfin Mako (MK), obtained from nanoindentation measurements in directions both parallel (top) and perpendicular (bottom) to the direction of biological strain of whole vertebrae. Each box plot displays minimum, first quartile, median, third quartile, maximum, and outliers. Empty circles represent outliers and empty squares represent the mean value in each the dataset. Means not sharing any letter are significantly different at the 5 % level of significance via post hoc Dunn test. Insets: schematics showing parallel (top) and perpendicular (bottom) direction of indentation.

expected parallel to the fiber direction [56]. Our PLM and AFM data have demonstrated that the collagen fiber orientation varies both locally as well as between species (Fig. S4). Despite the radial orientation of crystals in the corpus calcarea [51], this region shows a similarly high modulus of around 2 GPa in Shortfin Mako, surpassing all other tested regions in both shark species, which could be explained by its higher degree of calcification than in the intermedialia. In both the anterior and posterior region of the vertebral column, the unmineralized gaps of the Mako shark vertebrae are less stiff compared to that of the Blacktip shark when measured parallel and perpendicular to the major direction of biological strain. In both directions, the mean elastic moduli of the Blacktip shark are over twice that of the Mako shark. The relative homogeneity of the unmineralized region compared to the corpus calcarea and intermedialia is emphasized in the narrower spread of elastic modulus values obtained for this region of the vertebrae.

D. Raja Somu, M. Fuentes, L. Lou et al.

From previous bulk compression tests, we expected an increased stiffness in the tail of the lamnid Mako shark to support lateral body undulations [35]. However, we found that on the nanoscale, anterior mineralized vertebrae of the Mako shark appear stiffer, which could be due to several reasons: While the localized material properties of the anterior vertebrae are as such, its hierarchical arrangement, in comparison to the posterior vertebrae, could be sufficiently different to cause dramatic differences in its overall mechanical properties. It is known that the unmineralized portion of the vertebral cartilage is responsible for its extraordinary high yield point around 12 % strain, suggesting that shark vertebrae can deform dramatically before failure [12,14]. Additionally, it is possible, especially for the Mako shark, that whilst individ-

ual lamella, which were focus of this investigation, were less stiff along the tail, that their larger number in the posterior vertebrae contributes to radial reinforcement during bending and an even distribution of stress. This assumption is backed by a higher mineral content in posterior compared with anterior centra [12]. Additionally, the tail of the shark is instrumental in producing thrust in the swimming process compared to the anterior region of the body [57]. The Mako's thunniform swimming mode requires the body to remain stiff, while the tail is oscillating, whereas Blacktip sharks engage the entire body in undulatory movements during swimming. It is possible that the posterior region of the vertebral column therefore undergoes a more complex form of bending compared to the anterior region. Previous studies of leopard and bamboo sharks show that their heterocercal tail undergoes torsional bending and twisting that is crucial in the sharks' ability to make quick-turn maneuvers [58]. Since much of the movement in the shark species examined in this study are concentrated towards the posterior vertebrae, it is possible that applied stresses would be at least equal if not higher for the fast-swimming Blacktip and the even faster-swimming Mako. To meet these demands, it is feasible that the posterior region needs to be equipped to deal with multi-directional stresses that accompany torsional twisting movement that could occur during quick-swimming maneuvers.

Some variations in mechanical properties can also be attributed to overall differences in how distinct portions of the vertebral column are utilized during aquatic locomotion. In the undulatory swimming mode that propels Blacktip sharks, vertebrae are engaged in bending mode such that opposite sides of the centra undergo tension and compression. Studies have shown, however, that the tendons and musculature engaged in thunniform swimming

would keep the vertebrae closer to the tail under permanent compression, allowing for more powerful swimming [57,59].

The nanoindendation measurements in this portion of the study were conducted in Elasmobranch Ringer's solution to mimic the biological medium. The mechanical properties of soft biological tissues depend on the level of hydration and chemical environment (e.g. seawater or buffer) [60]. Indenting the sample in wet conditions was carried out since the results are closer to physiological conditions. In previous studies of mechanical characterization of cartilage in other systems (such as bovine articular cartilage), it was found that repeated thawing and freezing cartilage samples could somewhat affect their mechanical response [37,61,62]. However, due to the way in which samples are obtained and shipped, the relative scarcity of the samples, and the different capture dates for the sharks, freezing and thawing are unavoidable. To mitigate freezing artefacts, samples were, to the extent that they could be, left frozen as a whole centrum, without excision of arches and sheath, in order to minimize damage from ice crystals to the deeper cartilage. Regardless, we find these values starkly different enough from the macroscale stiffness of whole vertebrae that it warrants further study.

#### 3.5. General discussion

D. Raja Somu, M. Fuentes, L. Lou et al.

Previous macroscale mechanical testing studies have shown that the strain in the vertebral column that accompanies lateral bending is partially relaxed by the vertebrae themselves, and not simply by the intervertebral joints, and that the centra themselves play a mechanical role during aquatic locomotion [15]. Through an examination of the micro- and nanostructure of the shark vertebral cartilage matrix, we expand on current knowledge of the chemical composition and possible mechanical roles of the hierarchical organization of the vertebral centra.

We observed oriented fibril bundles in the unmineralized and mineralized portion of the Mako shark in PLM, and further examined them using AFM. It appears that while superficially similar on the microscale, there are ultrastructural differences in the mineralized and unmineralized regions with regards to fiber organization. In the mineralized region, for instance, the lacunae are aligned along the direction of the fibers, and elongations are oriented parallel to the fiber direction (Fig. S7). However, in the unmineralized region, there was more variety in the direction of the lacunae. This could suggest that the unmineralized gaps are better equipped to handle stress loaded in multiple directions compared to the intermedialia.

AFM and PLM confirm the major structural differences between the unmineralized region of the Blacktip shark and Mako shark. The presence of distributed fibrillar bundles and increased lacunae in Mako Shark could explain the lower elastic modulus of the unmineralized region of the Mako shark compared to that of the Blacktip shark, measured in the direction parallel to biological strain. The presence of these needle-like insertions could help dissipate local stress and therefore make for an overall less rigid material as the deformation spreads out over a larger area. In this way, we can link the microstructure of the different intravertebral regions to biomechanical differences observed. An examination of these bundles using polarized Raman microspectroscopy contributes further evidence as to the composition of these fiber bundles (Fig. S10).

Compositional variations within individual centra, which have not been the focus of the present study, could also contribute to the micromechanical properties of shark vertebral cartilage. For instance, Mako shark vertebrae has been shown to incorporate higher amounts of zinc across ontogeny compared to some Carchaniform species including Blacktip shark [63,64]. A study by Raoult et al. showed that the accumulation of strontium in the

vertebral cartilage of White Shark (Carcharodon carcharias) aligned more closely with traditionally assessed visual growth bands compared to calcium [65]. Zinc was found to be primarily deposited in the intermedialia and to a much smaller extent in the corpus calcarea [63]. As such, many previous studies on the elemental distribution in vertebral cartilage have focused on aging and environmental factors rather than potential influence on microstructure and mechanics. PLM, AFM, and Raman spectroscopic mappings from mineralized and unmineralized cartilage tissues reveal stark interspecies similarities and variations in structural morphology and fiber arrangement. PLM data indicates a preferred collagen fiber orientation in the unmineralized cartilage of Shortfin Mako, which was not observed in Blacktip cartilage tissue. Further investigations are necessary to shed light on the hierarchical collagen arrangement across shark species. Using Raman chemical mappings, we found an inverse relationship between GAG and mineral abundance and a lower degree of bioapatite crystallinity in the presence of GAGs, supporting their role in inhibiting apatite mineralization and cross-linking the organic matrix. In cartilaginous materials, collagen fibril bundles are thought to be the major tensile element, whereas bridging proteoglycans ensure that the tissue resists extensive compression and expands back to its original shape after load removal, but this aspect warrants further investigation. The intermedialia region in both species was interspersed with lacunar cartilage canals that either serve as a nutrient reservoir or distribute local stresses along the interface. In accordance with bulk compression tests from whole vertebral centra [35], it is evident that a larger mineral content correlates with higher vertebrae stiffness, yet little has been known about how individual structural elements contribute to the cartilage mechanics that dictate swimming styles and speeds employed among shark species. Macroscale and region-specific mechanical testing indicate that vertebral cartilage stiffness and strength depend on the abundance [14], distribution and orientation of bioapatite mineral. Based on nanomechanical testing, we conclude that the degree of mineralization is particularly relevant in the highly calcified corpus calcarean. We speculate that the thunniform swimming mode of Shortfin Mako sharks requires extraordinary stiffness in the anterior region of the vertebral column. The Carcharhiniform and Lamniform sharks studied here represent different mineralization morphologies, swimming styles and speeds, but given the limited number of species investigated, the conclusions cannot necessarily be extended to sharks in general. Using nanoindentation under near-native conditions, we found that Young's moduli from mineralized regions (corpus calcarean and intermedialia) are positively correlated with local mineral density. However, with values on the order of few GPa, local Young's moduli of the mineralized zones exceeded bulk measurements for whole vertebrae sections by a factor of 10 [35]. As expected from fiber-reinforced composites, the mechanical properties determined along the direction of biological strain were significantly higher than perpendicular to it. Intriguingly, unmineralized Blacktip shark cartilage was found to be substantially stiffer than Mako cartilage, which could be related to differences in the structural arrangement of the collagen fibers observed in PLM and AFM. In particular, the arrangement of fibers in the unmineralized regions of Mako centra and in the mineralized regions of Mako and Blacktip centra are reminiscent of discontinuous but aligned fiberreinforced composites, which generally have lower stiffness compared to composites with continuous unidirectional fibers in the main load direction [56]. It is possible that the lower stiffness associated with this kind of fiber arrangement adopted by this cartilage region is a tradeoff between mitigating crack propagation and handling multidirectional stresses.

Acta Biomaterialia xxx (xxxx) xxx

The biomechanics of the vertebral column reflect differences in ecological requirements, morphology, and behavior. Carcharhiniformes, such as Blacktip, are fast swimming, agile sharks that in-

JID: ACTBIO [m5G;October 14, 2024;16:53]

habit inshore and offshore waters, often nearshore around river mouths, bays, mangrove swamps, and estuaries [18–20]. Field observations found Blacktip sharks maneuver through shallow coastal waters to avoid predation [66]. Shortfin Makos, on the other hand, have adapted to engage in high-speed bursts and maintain high swimming speeds when migrating across oceans [67]. Furthermore, Blacktip and Mako sharks differ in steady-swimming kinematics: In non-lamnids, the wave of muscle activation tends to travel faster than the wave of muscle contraction, resulting in varying forces along the long body axis [68]. In lamnid sharks, such as Shortfin Mako, red muscle activation remains constant along the body, and red muscle shortening is synchronized with bending of

#### 4. Conclusions

posterior body parts [69].

D. Raja Somu, M. Fuentes, L. Lou et al.

Shark cartilage is a complex multi-scale composite material containing collagen type-II fibers, glucosaminoglycans, and carbonated apatite mineral. Previous research showed that the mineral content and macro-scale arrangement in mineralized vertebral cartilage greatly varies among species, among vertebrae in an individual shark, and along the length of the body [12,14,16]. In this study, we present a systematic and structured characterization of vertebral cartilage from typical Carcharhiniform and Lamniform shark species, Blacktip and Shortfin Mako, in which either mineralized blocks or radiating lamellae alternate with unmineralized regions, respectively. Based on our experimental data, intravertebral regiospecific micro- and nanoscale variations in mineralization patterns and chemical composition translate into different nanomechanical responses. We conclude that previously reported interspecies differences in bulk mechanical response are primarily attributed to the mineral content and microscale hierarchical arrangement of the mineralized regions. This in-depth microscopic and spectroscopic investigation provides deeper insights into the interplay between hard minerals and viscoelastic fibers in cartilage from the vertebral column, which may be related to the extraordinary speed of cartilaginous fish. Taken together, this study enhances our understanding of structure-function relationships in hierarchical biological materials, particularly the mechanical response of complex multi-component systems made from fibers and nanoparticles. By studying the intricacies of shark vertebrae, we hope to lay the foundation for biomimetic composite materials that harness lamellar reinforcement and tailored stiffness gradients, capable of dynamic and localized adjustments during movement.

#### **Declaration of competing interest**

The authors declare that they have no known competing financial interests or personal relationships that could have appeared to influence the work reported in this paper.

#### CRediT authorship contribution statement

**Dawn Raja Somu:** Writing – original draft, Visualization, Validation, Investigation, Formal analysis, Data curation. **Malena Fuentes:** Writing – review & editing, Formal analysis, Data curation. **Lihua Lou:** Writing – review & editing, Formal analysis, Data curation. **Arvind Agarwal:** Writing – review & editing, Resources. **Marianne Porter:** Writing – review & editing, Validation, Formal analysis. **Vivian Merk:** Writing – review & editing, Supervision, Project administration, Methodology, Funding acquisition, Conceptualization.

# Acknowledgments

Support from the National Science Foundation (DMR-2137663, Division of Materials Research) to Dr. Vivian Merk is kindly ac-

knowledged. Dr. Marianne Porter was supported by a National Science Foundation CAREER grant (NSF, IOS-1941713). We thank FAU's College of Engineering and Computer Science (COECS) and I-SENSE for joint seed funding to Dr. Merk and Dr. Porter. A part of this work was produced using the Bruker SkyScan 1173 micro-CT system at the Florida Atlantic University High School Owls Imaging Lab (RRID:SCR\_023805). We thank laboratory assistant Jamie Knaub for her assistance. We thank Dr. Michelle Passerotti and the Apex Predators Program/NEFSC Narragansett Lab of NOAA Fisheries and Jack Morris from the Sharks and Rays Conservation Research Program at Mote Marine Laboratory for vertebrae used in this study.

Acta Biomaterialia xxx (xxxx) xxx

# Supplementary materials

Supplementary material associated with this article can be found, in the online version, at doi:10.1016/j.actbio.2024.09.041.

#### References

- [1] U.G.K. Wegst, H. Bai, E. Saiz, A.P. Tomsia, R.O. Ritchie, Bioinspired structural materials, Nat. Mater. 14 (2015) 23–36.
- [2] B.S. Lazarus, A. Velasco-Hogan, T. Gómez-del Río, M.A. Meyers, I. Jasiuk, A review of impact resistant biological and bioinspired materials and structures, J. Mater. Res. Technol. 9 (2020) 15705–15738, doi:10.1016/j.jmrt.2020.10.062.
- [3] H. Mohammadi, Z. Ahmad, M. Petrů, S.A. Mazlan, M.A.F. Johari, H. Hatami, S.S.R. Koloor, An insight from nature: honeycomb pattern in advanced structural design for impact energy absorption, J. Mater. Res. Technol. 22 (2023) 2862–2887.
- [4] K. Tang, J. Xue, Y. Zhu, C. Wu, Design and synthesis of bioinspired nanomaterials for biomedical application, WIREs Nanomed. Nanobiotechnol. 16 (2024) e1914, doi:10.1002/wnan.1914.
- [5] A.C. do N. Pereira, S. Titotto, Bioinspired composites: nature's guidance for advanced materials future, Funct. Compos. Struct. 5 (2023) 12004, doi:10.1088/2631-6331/acbc64.
- [6] Q.-Q. Rong, Y.-H. Cui, T. Shimada, J.-S. Wang, T. Kitamura, Self-shaping of bioin-spired chiral composites, Acta Mech. Sin. 30 (2014) 533–539, doi:10.1007/s10409-014-0012-2.
- [7] M. Ilami, H. Bagheri, R. Ahmed, E.O. Skowronek, H. Marvi, Materials, actuators, and sensors for soft bioinspired robots, Adv. Mater. 33 (2021) 2003139, doi:10. 1002/adma.202003139.
- [8] L. Amorim, A. Santos, J.P. Nunes, J.C. Viana, Bioinspired approaches for toughening of fibre reinforced polymer composites, Mater. Des. 199 (2021) 109336, doi:10.1016/j.matdes.2020.109336.
- [9] I.J. Sansom, M.M. Smith, M.P. Smith, Scales of thelodont and shark-like fishes from the Ordovician of Colorado, Nature 379 (1996) 628-630, doi:10.1038/ 379628a0
- [10] P. Janvier, M. Arsenault, Calcification of early vertebrate cartilage, Nature 417 (2002) 609, doi:10.1038/417609a.
- [11] S. Rama, G. Chandrakasan, Distribution of different molecular species of collagen in the vertebral cartilage of shark (Carcharius acutus), Connect. Tissue Res. 12 (1984) 111–118, doi:10.3109/03008208408992776.
- [12] M.E. Porter, J.L. Beltrán, T.J. Koob, A.P. Summers, Material properties and biochemical composition of mineralized vertebral cartilage in seven elasmobranch species (Chondrichthyes), J. Exp. Biol. 209 (2006) 2920–2928.
- [13] J.J. Gelsleichter, J.A. Musick, P. Van Veld, Proteoglycans from the vertebral cartilage of the clearnose skate, Raja eglanteria: inhibition of hydroxyapatite formation, Fish Physiol. Biochem. 14 (1995) 247–251.
- [14] M.E. Porter, T.J. Koob, A.P. Summers, The contribution of mineral to the material properties of vertebral cartilage from the smooth-hound shark Mustelus californicus, J. Exp. Biol. 210 (2007) 3319–3327.
- [15] M.E. Porter, C. Diaz Jr, J.J. Sturm, S. Grotmol, A.P. Summers, J.H. Long Jr, Built for speed: strain in the cartilaginous vertebral columns of sharks, Zoology 117 (2014) 19–27.
- [16] W.G. Ridewood, E.W. MacBride, VIII.—On the calcification of the vertebral centra in sharks and rays, Philos. Trans. R. Soc. London. Ser. B, Contain. Pap. a Biol. Character. 210 (1921) 311–407.
- [17] L.J. Natanson, G.B. Skomal, S.L. Hoffmann, M.E. Porter, K.J. Goldman, D. Serra, Age and growth of sharks: do vertebral band pairs record age? Mar. Freshw. Res. 69 (2018) 1440-1452. doi:10.1071/MF17279.
- [18] L. Compagno, Sharks of the Order Carcharhiniformes, Blackburn Press, Caldwell. 2003.
- [19] L. Compagno, M. Dando, S. Fowler, Sharks of the World, 1st ed., Princeton University Press, Princeton, NY, 2005.
- [20] J.I. Castro, The Sharks of North America, Oxford University Press, New York, 2011.
- [21] M.E. Porter, B.T. Ruddy, S.M. Kajiura, Volitional swimming kinematics of blacktip sharks, carcharhinus limbatus, in the wild, Drones 4 (2020), doi:10.3390/ drones4040078.
- [22] P.A. Klimley, The Biology of Sharks and Rays, 1st ed., The University of Chicago Press, Chicago, 2013.

JID: ACTBIO [m5G;October 14, 2024;16:53]

[23] D. Bernal, D. Smith, G. Lopez, D. Weitz, T. Grimminger, K. Dickson, J.B. Graham, Comparative studies of high performance swimming in sharks II. Metabolic biochemistry of locomotor and myocardial muscle in endothermic and ectothermic sharks, J. Exp. Biol. 206 (2003) 2845–2857, doi:10.1242/jeb.00504.

D. Raja Somu, M. Fuentes, L. Lou et al.

- [24] M.R.H. Jeffrey, C. Carrier, John A. Musick, Biology of Sharks and Their Relatives, CRC Press, Boca Raton, 2012.
- [25] D. Xia, W. Chen, J. Liu, Z. Wu, Y. Cao, The three-dimensional hydrodynamics of thunniform swimming under self-propulsion, Ocean Eng. 110 (2015) 1–14, doi:10.1016/j.oceaneng.2015.10.008.
- [26] N.A. and O. Administration, Sharks That Can Be Legally Retained by Recreational Anglers in the Atlantic Ocean, Caribbean Sea and Gulf of Mexico, (n.d.).
- [27] S. Omelon, J. Georgiou, F. Variola, M.N. Dean, Colocation and role of polyphosphates and alkaline phosphatase in apatite biomineralization of elasmobranch tesserae, Acta Biomater. 10 (2014) 3899–3910, doi:10.1016/j.actbio.2014. 06.008
- [28] R. Seidel, M. Blumer, J. Chaumel, S. Amini, M.N. Dean, Endoskeletal mineralization in chimaera and a comparative guide to tessellated cartilage in chondrichthyan fishes (sharks, rays and chimaera), J. R. Soc. Interface 17 (2020) 20200474, doi:10.1098/rsif.2020.0474.
- [29] R. Seidel, A. Roschger, L. Li, J.J. Bizzarro, Q. Zhang, J. Yin, T. Yang, J.C. Weaver, P. Fratzl, P. Roschger, M.N. Dean, Mechanical properties of stingray tesserae: high-resolution correlative analysis of mineral density and indentation moduli in tessellated cartilage, Acta Biomater. 96 (2019) 421–435, doi:10.1016/j.actbio. 2019.06.038.
- [30] R. Seidel, K. Lyons, M. Blumer, P. Zaslansky, P. Fratzl, J.C. Weaver, M.N. Dean, Ultrastructural and developmental features of the tessellated endoskeleton of elasmobranchs (sharks and rays), J. Anat. 229 (2016) 681–702, doi:10.1111/joa. 12508
- [31] J.S. Park, H. Chen, K.C. James, L.J. Natanson, S.R. Stock, Three-dimensional mapping of mineral in intact shark centra with energy dispersive x-ray diffraction, J. Mech. Behav. Biomed. Mater. 136 (2022) 105506.
- [32] S.R. Stock, P.E. Morse, M.K. Stock, K.C. James, L.J. Natanson, H. Chen, P.D. Shevchenko, E.R. Maxey, O.A. Antipova, J.-S. Park, Microstructure and energy dispersive diffraction reconstruction of 3D patterns of crystallographic texture in a shark centrum, J. Med. Imaging 9 (2022) 31504.
- [33] S.R. Stock, P.E. Morse, M.K. Stock, K.C. James, L.J. Natanson, H. Chen, P.V. Shevchenko, E.R. Maxey, O. Antipova, J.S. Park, Microstructure and energy dispersive diffraction reconstruction of 3D patterns of crystallographic texture in shark centrum, Proc. SPIE (2021) 118400N, doi:10.1117/12.2595040.
- [34] S. R. Stock, U. Kierdorf, K. C. James, P. D. Shevchenko, L. J. Natanson, S. Gomez, H. Kierdorf, Acta Biomater. 177 (2024) 300–315.
- [35] D.I. Ingle, L.J. Natanson, M.E. Porter, Mechanical behavior of shark vertebral centra at biologically relevant strains, J. Exp. Biol. 221 (2018) jeb188318.
- [36] L. Maheo, P. Viot, D. Bernard, A. Chirazi, G. Ceglia, V. Schmitt, O. Mondain-Monval, Elastic behavior of multi-scale, open-cell foams, Compos. Part B Eng. 44 (2013) 172–183, doi:10.1016/j.compositesb.2012.06.006.
- [37] J. Chaumel, M. Marsal, A. Gómez-Sánchez, M. Blumer, E.J. Gualda, A. de Juan, P. Loza-Alvarez, M.N. Dean, Autofluorescence of stingray skeletal cartilage: hyperspectral imaging as a tool for histological characterization, Discov. Mater. 1 (2021) 16, doi:10.1007/s43939-021-00015-x.
- [38] G. Penel, G. Leroy, C. Rey, E. Bres, MicroRaman spectral study of the PO4 and CO3 vibrational modes in synthetic and biological apatites, Calcif. Tissue Int. 63 (1998) 475–481, doi:10.1007/s002239900561.
- [39] M. López-Álvarez, E. López-Senra, J. Valcárcel, J.A. Vázquez, J. Serra, P. González, Quantitative evaluation of sulfation position prevalence in chondroitin sulphate by Raman spectroscopy, J. Raman Spectrosc. 50 (2019) 656– 664, doi:10.1002/jrs.5563.
- [40] N. Prokopi, K.S. Andrikopoulos, A.S. Beobide, G.A. Voyiatzis, D.J. Papachristou, Collagen orientation probed by polarized Raman spectra can serve as differential diagnosis indicator between different grades of meniscus degeneration, Sci. Rep. 11 (2021) 20299, doi:10.1038/s41598-021-99569-2.
- [41] N.S.J. Lim, Z. Hamed, C.H. Yeow, C. Chan, Z. Huang, Early detection of biomolecular changes in disrupted porcine cartilage using polarized Raman spectroscopy, J. Biomed. Opt. 16 (2011) 17003.
- [42] M. López-Álvarez, P. González, J. Serra, J. Fraguas, J. Valcarcel, J.A. Vázquez, Chondroitin sulfate and hydroxyapatite from Prionace glauca shark jaw: physicochemical and structural characterization, Int. J. Biol. Macromol. 156 (2020) 329–339, doi:10.1016/j.ijbiomac.2020.04.010.
- [43] M.S. Bergholt, J.-P. St-Pierre, C.S. Offeddu, P.A. Parmar, M.B. Albro, J.L. Puetzer, M.L. Oyen, M.M. Stevens, Raman spectroscopy reveals new insights into the zonal organization of native and tissue-engineered articular cartilage, ACS Cent. Sci. 2 (2016) 885–895.
- [44] J.J. Cárcamo, A.E. Aliaga, R.E. Clavijo, M.R. Brañes, M.M. Campos-Vallette, Raman study of the shockwave effect on collagens, Spectrochim. Acta Part A Mol. Biomol. Spectrosc. 86 (2012) 360–365, doi:10.1016/j.saa.2011.10.049.
- [45] B. Wopenka, A. Kent, J.D. Pasteris, Y. Yoon, S. Thomopoulos, The tendon-to-bone transition of the rotator cuff: a preliminary raman spectroscopic study documenting the gradual mineralization across the insertion in rat tissue samples, Appl. Spectrosc. 62 (2008) 1285–1294 https://opg.optica.org/as/abstract.cfm?URI=as-62-12-1285.

[46] M. Takagi, R.T. Parmley, F.R. Denys, M. Kageyama, Ultrastructural visualization of complex carbohydrates in epiphyseal cartilage with the tannic acid-metal salt methods, J. Histochem. Cytochem. 31 (1983) 783–790, doi:10.1177/31.6. 6188782.

Acta Biomaterialia xxx (xxxx) xxx

- [47] S.G. Rees, D.T. Hughes Wassell, G. Embery, Interaction of glucuronic acid and iduronic acid-rich glycosaminoglycans and their modified forms with hydroxyapatite, Biomaterials 23 (2002) 481–489, doi:10.1016/S0142-9612(01) 00130-2.
- [48] D. R. Keene and S. F. Tufa, in *Electron Microscopy of Model Systems*, ed. T. B. T.-M. in C. B. Müller-Reichert, Academic Press, 2010, vol. 96, pp. 443–473.
- [49] J.M. Hoenig, A.H. Walsh, The occurrence of cartilage canals in shark vertebrae, Can. J. Zool. 60 (1982) 483–485, doi:10.1139/z82-069.
- [50] P.E. Morse, M.K. Stock, K.C. James, L.J. Natanson, S.R. Stock, Shark centra microanatomy and mineral density variation studied with laboratory microComputed tomography, J. Struct. Biol. 214 (2022) 107831, doi:10.1016/j.jsb.2022. 107831.
- [51] J.S. Park, J.D. Almer, K.C. James, L.J. Natanson, S.R. Stock, Bioapatite in shark centra studied by wide-angle and by small-angle X-ray scattering, J. R. Soc. Interface 19 (2022) 20220373, doi:10.1098/rsif.2022.0373.
- [52] T. Ishimoto, T. Nakano, Y. Umakoshi, M. Yamamoto, Y. Tabata, Degree of biological apatite c-axis orientation rather than bone mineral density controls mechanical function in bone regenerated using recombinant bone morphogenetic protein-2, J. Bone Miner. Res. 28 (2013) 1170–1179, doi:10.1002/jbmr.1825.
- [53] T. Nakano, K. Kaibara, Y. Tabata, N. Nagata, S. Enomoto, E. Marukawa, Y. Umakoshi, Unique alignment and texture of biological apatite crystallites in typical calcified tissues analyzed by microbeam x-ray diffractometer system, Bone 31 (2002) 479–487, doi:10.1016/S8756-3282(02)00850-5.
- [54] R. Ozasa, T. Ishimoto, S. Miyabe, J. Hashimoto, M. Hirao, H. Yoshikawa, T. Nakano, Osteoporosis changes collagen/apatite orientation and young's modulus in vertebral cortical bone of rat, Calcif. Tissue Int. 104 (2019) 449–460, doi:10.1007/s00223-018-0508-z.
- [55] Y. Otsuka, J. Tatami, I. Yamamoto, M. Iijima, T. Ohji, Micro- and macro-scale strength properties of c-axis aligned hydroxyapatite ceramics, Ceram. Int. 49 (2023) 40158–40165, doi:10.1016/j.ceramint.2023.09.349.
- [56] H.W. Wang, H.W. Zhou, L.L. Gui, H.W. Ji, X.C. Zhang, Analysis of effect of fiber orientation on Young's modulus for unidirectional fiber reinforced composites, Compos. Part B Eng. 56 (2014) 733–739, doi:10.1016/j.compositesb.2013.09.020.
- [57] S. Gemballa, P. Konstantinidis, J.M. Donley, C. Sepulveda, R.E. Shadwick, Evolution of high-performance swimming in sharks: transformations of the musculotendinous system from subcarangiform to thunniform swimmers, J. Morphol. 267 (2006) 477–493, doi:10.1002/jmor.10412.
- [58] C.D. Wilga, G.V. Lauder, Function of the heterocercal tail in sharks: quantitative wake dynamics during steady horizontal swimming and vertical maneuvering, J. Exp. Biol. 205 (2002) 2365–2374, doi:10.1242/jeb.205.16.2365.
- [59] J.M. Donley, C.A. Sepulveda, P. Konstantinidis, S. Gemballa, R.E. Shadwick, Convergent evolution in mechanical design of lamnid sharks and tunas, Nature 429 (2004) 61–65, doi:10.1038/nature02435.
- [60] L. Lou, L. Paolino, A. Agarwal, Bridging the gap in Ashby's map for soft material properties for tissue engineering, ACS Appl. Mater. Interfaces 15 (2023) 24197– 24208, doi:10.1021/acsami.3c04331.
- [61] A.E. Peters, E.J. Comerford, S. Macaulay, K.T. Bates, R. Akhtar, Micromechanical properties of canine femoral articular cartilage following multiple freeze-thaw cycles, J. Mech. Behav. Biomed. Mater. 71 (2017) 114–121, doi:10.1016/j.jmbbm. 2017.03.006
- [62] M. Szarko, K. Muldrew, J.E.A. Bertram, Freeze-thaw treatment effects on the dynamic mechanical properties of articular cartilage, BMC Musculoskelet. Disord. 11 (2010) 231, doi:10.1186/1471-2474-11-231.
- [63] V. Raoult, N. Howell, D. Zahra, V.M. Peddemors, D.L. Howard, M.D. de Jonge, B.L. Buchan, J.E. Williamson, Localized zinc distribution in shark vertebrae suggests differential deposition during ontogeny and across vertebral structures, PLoS ONE 13 (2018) e0190927, doi:10.1371/journal.pone.0190927.
- [64] M.C. Livernois, J.A. Mohan, T.C. TinHan, T.M. Richards, B.J. Falterman, N.R. Miller, R.J.D. Wells, Ontogenetic patterns of elemental tracers in the vertebrae cartilage of coastal and oceanic sharks, Front. Mar. Sci. 8 (2021) https: //www.frontiersin.org/article/10.3389/fmars.2021.704134.
- [65] V. Raoult, V.M. Peddemors, D. Zahra, N. Howell, D.L. Howard, M.D. de Jonge, J.E. Williamson, Strontium mineralization of shark vertebrae, Sci. Rep. 6 (2016) 29698, doi:10.1038/srep29698.
- [66] M.D. Doan, S.M. Kajiura, Adult blacktip sharks (Carcharhinus limbatus) use shallow water as a refuge from great hammerheads (Sphyrna mokarran), J. Fish Biol. 96 (2020) 1530–1533, doi:10.1111/jfb.14342.
- [67] B.M. Saraiva, B.C.L. Macena, S. Solleliet-Ferreira, P. Afonso, J. Fontes, First insights into the shortfin make shark (Isurus oxyrinchus) fine-scale swimming behaviour, R. Soc. Open Sci. 10 (2023) 230012, doi:10.1098/rsos.230012.
- [68] R.E. Shadwick, J.A. Goldbogen, Muscle function and swimming in sharks, J. Fish Biol. 80 (2012) 1904–1939, doi:10.1111/j.1095-8649.2012.03266.x.
- [69] J.M. Donley, R.E. Shadwick, C.A. Sepulveda, P. Konstantinidis, S. Gemballa, Patterns of red muscle strain/activation and body kinematics during steady swimming in a lamnid shark, the shortfin mako (Isurus oxyrinchus), J. Exp. Biol. 208 (2005) 2377–2387, doi:10.1242/jeb.01618.